Burial Ages Imply Miocene Uplift of Lu Mountain in East China due to Crustal Shortening

Zhiyong Han, Rouxian Pan, Xusheng Li*, Yujia Liu, Yufang Li and Xianyan Wang

School of Geography and Ocean Science, Nanjing University, Nanjing, China

Confined by the eastern and western boundary faults, Lu Mountain has long been considered a block mountain uplifted due to Mesozoic and Cenozoic crustal deformation in East China. However, the formation and evolution of this block mountain are still debated. In this study, the eastern boundary fault is investigated to confirm the tectonic style of the block mountain. In addition, the burial ages of sediments on the fans of the eastern piedmont are measured by $^{26}Al/^{10}Be$ dating to evaluate the denudation rate. Field evidence indicates the presence of a reverse fault (Xingzi reverse fault) acting as the eastern boundary fault, which demonstrates that the block mountain is not a horst as once thought but an extrusion structure. Corrected $^{26}Al/^{10}Be$ burial ages show that the sediments on the high-level fans were deposited at approximately 1.1–1.2 Ma, which indicates denudation rates ranging from 0.033 to 0.082 m/kyr. The vertical displacement along the Xingzi reverse fault is estimated to be at least 1,100 m. The hanging wall could have been eroded to its present position within 13–33 Myr at the above denudation rates. Combining our results with regional geological and geomorphological evidence, we suggest that Lu Mountain was mainly uplifted in the Miocene due to crustal compression deformation, which may have been a response to the movement of the Pacific plate.

Keywords: Lu mountain, block mountain, extrusion structure, denudation rate, burial age

INTRODUCTION

Determining the time and amplitude of the tectonic uplift of mountains is an important research topic in tectonics and geomorphology (e.g., Tapponnier et al., 2001; Wang et al., 2008; Fang et al., 2020). Tectonic uplift has been explored through low-temperature thermochronology (Clark et al., 2010), cosmogenic nuclide-derived ages and erosion rates (Palumbo et al., 2011) and fault scarp heights (Zheng et al., 2013). Among these approaches, denudation rates are now receiving increasing attention since they can imply tectonic movement and climate change (Reiners and Brandon, 2006) and can be used to determine the time of tectonic uplift together with independent geomorphic markers (Palumbo et al., 2009; Yuan et al., 2011).

East China, located at the junction of the Eurasian, Indo-Australian and Pacific plates, has experienced complex transformation processes under various tectonic systems and regimes (Li et al., 2013). The Mesozoic and Cenozoic tectonic deformation has shaped the modern geomorphic outline. Therefore, studying the development and evolution of modern landforms contributes to revealing the Mesozoic and Cenozoic tectonic deformation and tectono-dynamic background. At

present, mountains and basins in East China have become important research objects in tectonics (Shu and Wang, 2006; Xu et al., 2014; Suo et al., 2017).

Lu Mountain is the only region on the southeastern margin of the South China block where the Precambrian crystalline basement with a high degree of metamorphism is exposed (Guan et al., 2010), forming a crucial "window" to provide insight into the Jiangnan orogenic belt and the South China block. Lu Mountain has long been considered a horst, and the uplifted side is composed of Sinian and pre-Sinian metamorphic rocks (Fang, 1959). However, this author did not illustrate the exact positions of Lu Mountain's boundary faults. Since then, the idea that Lu Mountain is geologically a horst has become widespread. It has also been considered a klippe (Hsu et al., 1988); however, no thrust fault leading to northwestward movement of Lu Mountain has been found. A metamorphic core complex was suggested in a later study to have formed due to crustal extensional deformation during a period from the end of the Mesozoic to the beginning of the Cenozoic (Xiang et al., 1993). Subsequently, this view was questioned because the geological structure in Lu Mountain is obviously different from that of a metamorphic core complex (Yin and Xie, 1996; Bi et al., 1998). A recent study further found that the Xingzi Group is not the oldest metamorphic core, which undermines the interpretation of a metamorphic core complex (Wang et al., 2013).

The tectonic style of Lu Mountain remains undetermined, hindering a better understanding of its formation. This dilemma is largely due to the unclear nature of the Lu Mountain boundary faults. Early studies suggested that the Wuli normal fault is the eastern boundary fault based only on the study of drill cores at Wuli (Xiang et al., 1993). However, the existence of the Wuli normal fault has not been confirmed by other studies. Therefore, the eastern boundary fault becomes the key to determining the tectonic pattern and geo-morphogenesis of Lu Mountain.

Due to the lack of direct dating data, the uplift process of Lu Mountain remains controversial. The earliest study suggested that the mountain was uplifted at the end of the Neogene or the beginning of the Quaternary (Ren, 1953). A later study proposed that Lu Mountain has been intermittently uplifted since the end of the Neogene (Li and Zhu, 1987). Another study reported that Lu Mountain experienced strong uplift in the Pleistocene (Liu, 1987). The formation of Lu Mountain has also been divided into an initial stage in the late Permian- Palaeogene/Neogene and a formative stage in the late Neogene-Quaternary (Bi et al., 1996). In contrast to the above views, Lu Mountain was thought to have been uplifted in the middle Pleistocene (Peng and Huang, 1982; Zhu, 1995). Based on the calculation of stream steepness, the uplift of Lu Mountain was found to be slow in the early stage and fast in the late stage (Wang et al., 2015; Han et al., 2017).

To determine the pattern and the processes of the tectonic uplift of Lu Mountain, we carried out a field investigation of the eastern boundary fault. The burial ages of deposits on the eastern piedmont of Lu Mountain were measured by the $^{26}Al/^{10}Be$ method, and the denudation rates were calculated accordingly. Then, the denudation time of the uplifted side was estimated to define the approximate age of tectonic uplift. Combining these results with other evidence, a new tectonic pattern for Lu Mountain is proposed. Our study can help to better understand the formation and evolution of Mesozoic-Cenozoic mountains and basins in East China.
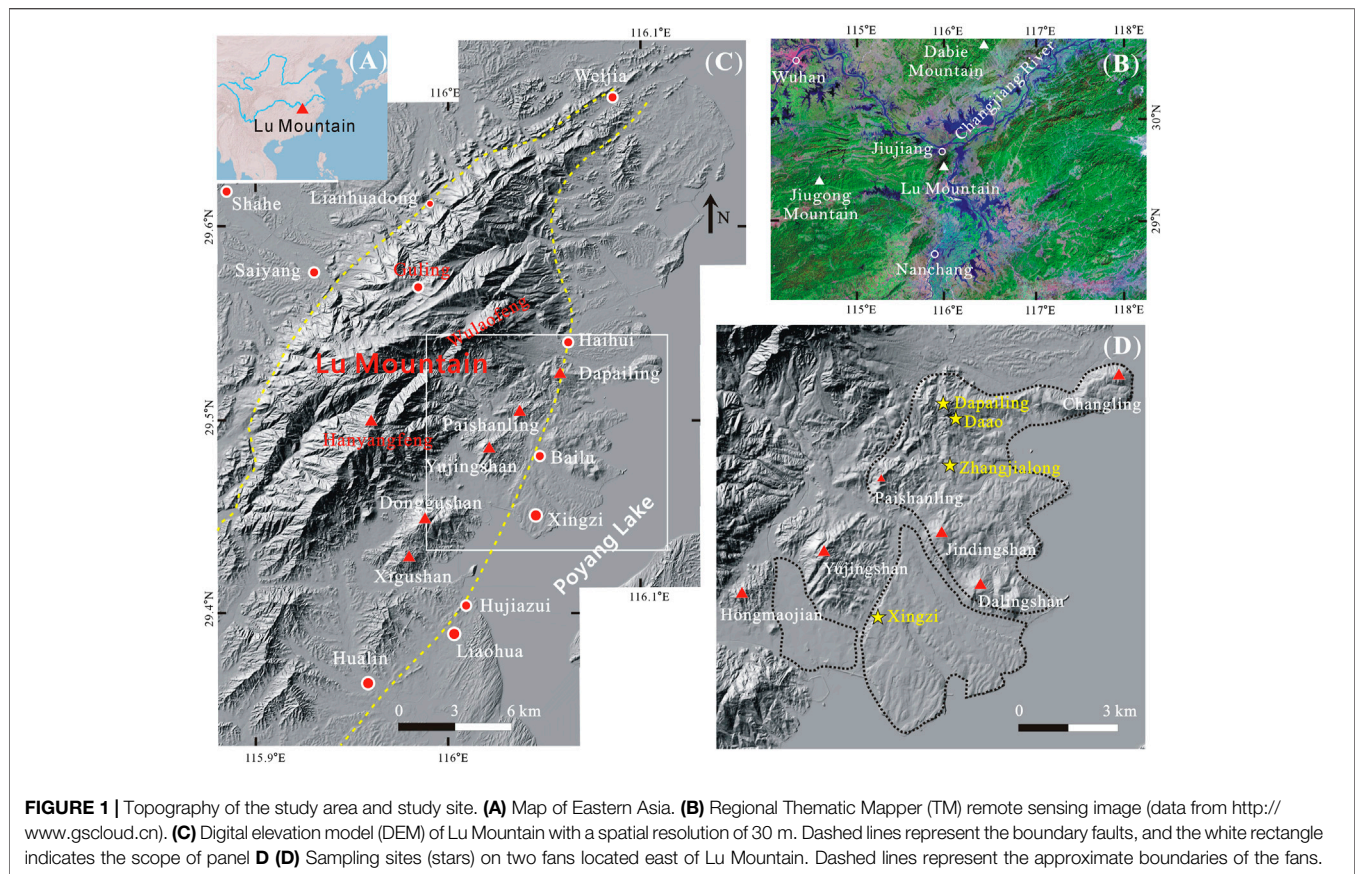
GENERAL BACKGROUND

Geomorphological Characteristics

Lu Mountain is located in Jiujiang city, Jiangxi Province, with the Changjiang River flowing on the northern side and Poyang Lake lying on the eastern side (**Figures 1A,B**). From a bird's-eye view, Lu Mountain looks like a spindle extending NE-SW with a length of approximately 33 km and a width in the middle of 10 km (**Figure 1C**). Lu Mountain reaches 1,473 m above sea level (a.s.l.), and the elevations of most peaks are close to 1,300 m a.s.l. A youthful topography represented by V-shaped valleys is well developed on the massif margin, while a mature topography represented by wide valleys is distributed in the central area of the massif (Ren, 1953). The mature topography of Lu Mountain was suggested to have formed in the Neogene and been uplifted to its present elevation by neotectonic movement (Li and Zhu, 1987). Tectonic uplift led to a decrease in the base level of erosion and headward erosion of streams rising on Lu Mountain. The knickpoints generated by headward erosion are generally located at elevations of 1,000–1,300 m a.s.l. (Wang et al., 2015). The mature topography survives where headward erosion has not yet arrived.

Geological Setting

Lu Mountain is situated at the junction of the middle and lower Yangtze plates, with a Mesozoic collisional orogenic belt (Dabie Mountain) in the north and a Neoproterozoic Jiangnan orogenic belt in the south (Zhu et al., 2010). Lu Mountain is located at the northern end of the Ganjiang fault, which can be regarded as the southern extension of the Tanlu fault (Wu et al., 2007). The metamorphic rocks with the highest metamorphic grade in this area appear on the southeastern piedmont of Lu Mountain and constitute the Xingzi Group, which is mainly distributed in an elliptical area with the long axis passing through Donggushan and Yujingshan (**Figure 2**). The Xingzi Group was intruded by Mesozoic magmas, forming the biotite granite at Donggushan, the granodiorite at Haihui, and the light-coloured granite at Wuli (Lin et al., 2000). The U-Pb age of detrital zircons obtained by secondary ionization mass spectrometry (SIMS) in leptite from the Xingzi Group is 834 ± 4 Ma, indicating that the Xingzi Group belongs to the Neoproterozoic (Guan et al., 2010).

The block mountain can be divided into southern and northern parts by a line from Litoujian to Jiuqifeng. The southern mountain has outcrops of the Shuangqiaoshan Group and Lushanlong Group (Xie et al., 1996). The sensitive high-resolution ion microprobe (SHRIMP) U-Pb age of zircons in spilite from the Lushanlong Group is 840 ± 6 Ma, and the U-Pb age of zircons in rhyolite is approximately 830 Ma (Gao et al., 2012). The SHRIMP U-Pb age of zircons from the Lushanlong Group is 838 ± 4 Ma (Shi et al., 2014). Hence, the Lushanlong Group belongs to the Neoproterozoic (**Figure 3**). The sandstone

FIGURE 1 | Topography of the study area and study site. **(A)** Map of Eastern Asia. **(B)** Regional Thematic Mapper (TM) remote sensing image (data from http://www.gscloud.cn). **(C)** Digital elevation model (DEM) of Lu Mountain with a spatial resolution of 30 m. Dashed lines represent the boundary faults, and the white rectangle indicates the scope of panel **D (D)** Sampling sites (stars) on two fans located east of Lu Mountain. Dashed lines represent the approximate boundaries of the fans.

and quartzite intercalated with phyllite in the Liantuo Formation of the Nanhua System are mainly exposed in the northern mountains (Han et al., 2017).

The Nanhua System is seldom exposed on the southwest piedmont of Lu Mountain. Sinian rocks crop out on the western and northeast piedmont. Lower Palaeozoic rocks are mainly exposed outside the massif. Generally, the strata tend to become younger with increasing distance from the massif. The upper Palaeozoic is found in southwestern Shahe. The upper Cretaceous Hekou Formation (Nanxiong Formation) is sporadically exposed near the shore of Poyang Lake. The Palaeocene Miaoling Formation forms scattered outcrops in the northwest. Quaternary deposits are widely distributed, especially in the piedmont and peripheral areas, with complex lithologies and multiple genetic types.

Lu Mountain can be regarded as a dome or brachy-anticline (referred to as the Lu anticline), but the Xingzi Group does not occupy the hinge of the brachy-anticline (Lin et al., 2000). Two distinct tectonic-metamorphic-magmatic events are revealed on Lu Mountain. The D2 event corresponds to the formation of the brachy-anticline extending NE-SW. Syntectonic granodiorite indicates that fold deformation occurred at 127 Ma. The D3 event manifests as a 6-km-long ductile shear zone in leucogranite, and surrounding rocks can be seen on the eastern piedmont. The shear zone consists of sinistral normal faults extending NNE-SSW and contemporaneous with the

emplacement of leucogranite at 100–110 Ma (Lin et al., 2000). Sinistral ductile shear zones extending NNE-SSW on the southeastern piedmont have been found (Xie et al., 1996), which may also be products of the D3 event. The western boundary fault is called the Lianhuandong normal fault, while the eastern boundary fault passes Haihui, Wuli and Hualin (**Figure 2**) and was once recognized as a normal fault (Xiang et al., 1993).

DATA AND METHODS

Geological and Topographical Data

The geological data for northern Jiangxi Province were derived from the 1:1,500,000 geological map (Ma, 2002), and those of Lu Mountain were obtained from the 1:50,000 geological maps and the auxiliary instructions produced by the Jiangxi Bureau of Geology and Mineral Resources (JBGMR), including Lushan region (Jiangxi Bureau of Geology and Mineral Resources, 1993a), Haihui region (Jiangxi Bureau of Geology and Mineral Resources, 1993b), Mahuiling region (Jiangxi Bureau of Geology and Mineral Resources, 1995a) and Xingzi region (Jiangxi Bureau of Geology and Mineral Resources, 1995b).

A 1:10,000 digital topographic map of Lu Mountain was provided by the Jiangxi Bureau of Surveying and Mapping. Then, a 5-m digital elevation model (DEM) was generated.
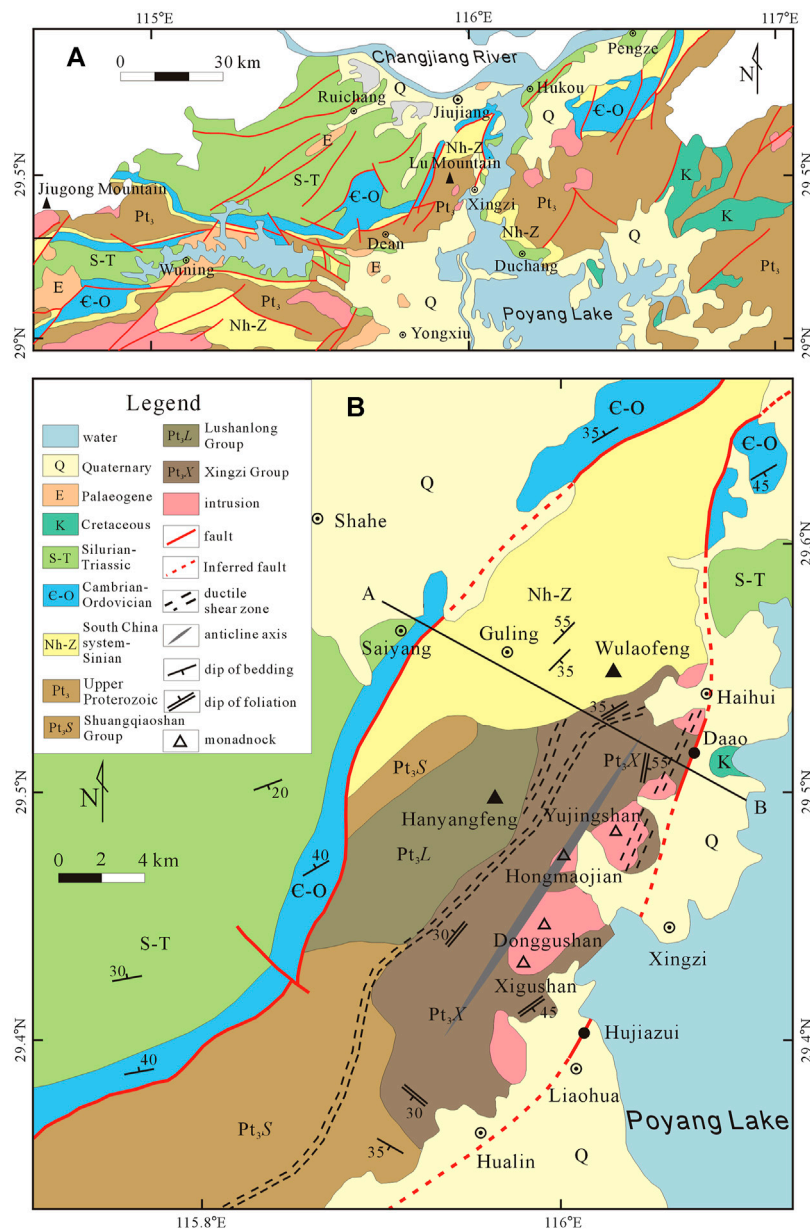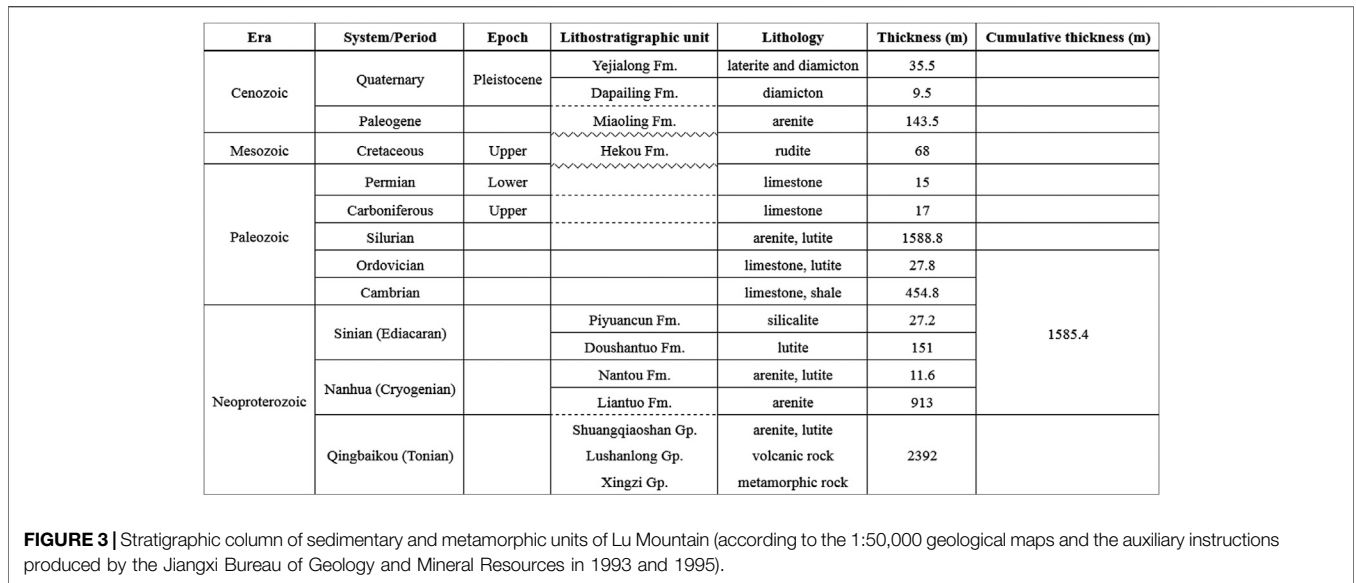
FIGURE 2 | Simplified geological map **(A)** Regional geological map modified after the geological map of Jiangxi Province (Ma, 2002). **(B)** Geological map of Lu Mountain (modified after the 1:50,000 geological maps produced by the Jiangxi Bureau of Geology and Mineral Resources in 1993 and 1995). Line A-B indicates the position of the cross-section in **Figure 7**.

This DEM has a mean elevation error of ±1.7 m in the hill area, ± 3.3 m in the mountain area. Each site was positioned using a GPS navigator in the field, further marked in the DEM according to the latitude and longitude and examined in the Google Earth. The elevation of each site was measured in DEM, which was used for further analysis.

Estimation of Denudation Rate

The denudation rate on the piedmont is estimated from perched sediments. Alluvial and debris flow sediments are usually accumulate on the bottoms of valleys on the piedmont. When the piedmont is denudated, valleys undergo gradual down-cutting. The denudation thickness is approximately equal to the relief between the modern valley bottom and the perched sediments. The duration of denudation approximates the sedimentary ages. Hence, the denudation rate can be estimated by dividing the relief by the sedimentary ages. Certainly, the estimated value represents only the average denudation rate since the deposition. Uneven denudation may result in spatially variable denudation rates. Therefore, the measurements have to be made on multiple locations to obtain a regionally representative denudation rate. The sedimentary age can be

Era	System/Period	Epoch	Lithostratigraphic unit	Lithology	Thickness (m)	Cumulative thickness (m)
Cenozoic	Quaternary	Pleistocene	Yejialong Fm.	laterite and diamicton	35.5	
	Quaternary	Pleistocene	Dapailing Fm.	diamicton	9.5	
	Paleogene		Miaoling Fm.	arenite	143.5	
Mesozoic	Cretaceous	Upper	Hekou Fm.	rudite	68	
Paleozoic	Permian	Lower		limestone	15	
	Carboniferous	Upper		limestone	17	
	Silurian			arenite, lutite	1588.8	
	Ordovician			limestone, lutite	27.8	
	Cambrian			limestone, shale	454.8	
Neoproterozoic	Sinian (Ediacaran)		Piyuancun Fm.	silicalite	27.2	
			Doushantuo Fm.	lutite	151	1585.4
	Nanhua (Cryogenian)		Nantou Fm.	arenite, lutite	11.6	
			Liantuo Fm.	arenite	913	
	Qingbaikou (Tonian)		Shuangqiaoshan Gp.	arenite, lutite	2392	
			Lushanlong Gp.	volcanic rock		
			Xingzi Gp.	metamorphic rock		

FIGURE 3 | Stratigraphic column of sedimentary and metamorphic units of Lu Mountain (according to the 1:50,000 geological maps and the auxiliary instructions produced by the Jiangxi Bureau of Geology and Mineral Resources in 1993 and 1995).

determined by the ^{26}Al/^{10}Be dating method if the sediments have been buried deeply enough.

The obtained values may represent earlier denudation rates if the terrain and environments have not changed significantly. If the earlier denudation thickness is known, dividing the denudation thickness by the denudation rate yields the denudation time. Because the denudation takes place on elevated terrains, the denudation time may indicate the time of the terrain uplift. In this study, this approach is used to estimate the onset time of the Lu Mountain uplift.

^{26}Al/^{10}Be Dating Method

The basic principle of the ^{26}Al/^{10}Be burial dating method is that rocks on the surface bombarded by cosmic rays can produce the cosmogenic radionuclides ^{26}Al and ^{10}Be, and the production rate ratio of ^{26}Al to ^{10}Be is approximately 6.8. When the rock is covered, the production rates of ^{26}Al and ^{10}Be decay exponentially with depth. Due to the faster decay of ^{26}Al, the ratio of ^{26}Al to ^{10}Be decreases with time. By measuring the ratio of ^{26}Al to ^{10}Be in the sample, we can calculate the burial age of rocks.

When the burial depth is insufficient, ^{26}Al and ^{10}Be will continue to be produced in the sample. Therefore, the total ^{26}Al and ^{10}Be contents change with time following the formulas below:

$$\left(N_{26} - N_{26,pb}\right) / \left(N_{10} - N_{10,pb}\right) = R_{inh}e^{-t/\tau_{\text{bur}}} \quad (1)$$

$$\tau_{bur} = 1 / \left(1/\tau_{26} - 1/\tau_{10}\right) \quad (2)$$

$$R_{inh} = \left(N_{26,\,inh} / N_{10,\,inh}\right) \quad (3)$$

N_{26} and N_{10} are the measured contents of ^{26}Al and ^{10}Be in the sample. $N_{26,pb}$ and $N_{10,pb}$ are the contents of ^{26}Al and ^{10}Be generated after burial, while $N_{26,\,inh}$ and $N_{10,\,inh}$ are the contents of ^{26}Al and ^{10}Be generated before burial. The average lifetime of ^{26}Al (τ_{26}) is 1.03 ± 0.02 Ma, and the average lifetime of ^{10}Be (τ_{10}) is 2.005 ± 0.02 Ma, and t means burial age.

If the burial depth is sufficient, the generation of ^{26}Al and ^{10}Be after burial can be ignored, and the formula can then be simplified as:

$$N_{26}/N_{10} = R_{inh}e^{-t/\tau_{\text{bur}}} \quad (4)$$

In this formula, only R_{inh} is unknown and can usually be calculated by the following formulas:

$$N_{26}/N_{10} = \left(P_{26}/P_{10}\right)\left(1 + N_{10}^*\right) \quad (5)$$

$$N_{10}^* = N_{10} / \left(P_{10}\tau_{10}\right) \quad (6)$$

$$N_{26}/N_{10} = \left[\left(P_{26}/P_{10}\right) / \left(1 + N_{10}^* e^{t/\tau_{10}}\right)\right]e^{-t/\tau_{\text{bur}}} \quad (7)$$

$$t \approx \tau^* ln\left[-\frac{1}{2N_{10}^*} + \sqrt{\left(\frac{1}{2N_{10}^*}\right)^2 + \frac{2}{N_{26}^*}}\right] \quad (8)$$

τ^* is 2.04 Ma, which is the average value of τ_{10} and τ_{bur}. In the formula, t is also called the minimum age of the sample. The above formula is applicable to rapidly and deeply buried samples after their exposure at the surface. If a sample has experienced a complex exposure history, the obtained age should be regarded as the upper limit of the actual age (Granger and Muzikar, 2001).

Preferably, the vertical and horizontal burial depths of samples should be greater than 20 and 10 m, respectively (Kong, 2012). If the burial depth is insufficient, the corrected age of the sample, also known as the maximum age, should be calculated according to the burial depth and the average density of the overlying sediments (2.0 g/cm^3 is used in this paper). According to longitude, latitude and elevation, we calculated the production rates of ^{26}Al and ^{10}Be by using the online program CRONUS-Earth (http://hess.ess.washington.edu/math/). The production rate of ^{10}Be (P_{10}) at a certain depth can be approximated by using the sum of four exponentials (Granger and Smith, 2000).

$$P_{10} = \sum_{j} A_{10,j}e^{-z/L_j} \quad (9)$$

$A_{10,j}$ and L_j represent the production rate factor and penetration length factor, respectively (Granger et al., 2014), z is the depth, and j represents each exponential equation. Then, according to the ratio of 6.8, the production rate of ^{26}Al at the same depth can be calculated. We can substitute the minimum age into formula (10) to calculate the contents of $N_{26,pb}$ and $N_{10,pb}$ after burial.

$$N_{i,pb} = P_{pb}\tau_i \left(1 - e^{-t/\tau_i}\right) \tag{10}$$

The measured contents minus $N_{26,pb}$ and $N_{10,pb}$ yield $N_{26,\,inh}$ and $N_{10,\,inh}$. When putting these values into formula (8), a new age is available. After many iterations, the corrected age can finally be obtained. The dating range of this method is 0.1–5.0 Ma (Granger and Muzikar, 2001). If the overlying strata of the buried sample accumulate slowly or undergo significant erosion, the corrected age will be biased.

Quartz is the most suitable mineral for ^{26}Al/^{10}Be burial dating because quartz is a stable mineral on the surface and easily forms a closed system. In addition, the ^{27}Al content of quartz is very low, which is conducive to accurate measurement of ^{26}Al. Approximately 30 quartz gravels were collected in the field. First, the sample was etched for 40 min by using 38% HF to remove the surface layer that might be contaminated. After rinsing and drying, gravels were pulverized, and the impure particles were removed. Finally, 0.25–0.5 mm quartz particles were obtained. To test the purity of quartz samples, measuring the aluminum content was necessary. Samples with Al contents below 100 ppm are generally accepted as pure (Kong, 2012). The Al content of each 0.5 g subsample was measured by using inductively coupled plasma optical emission spectroscopy (ICP-OES) in the Analysis and Testing Center of Nanjing Normal University. The qualified quartz samples were sent to the Purdue Rare Isotope Measurement (PRIME) Laboratory at Purdue University for chemical separation, target preparation and accelerator mass spectrometry (AMS) measurement of Al and Be.

RESULTS

Xingzi Reverse Fault

The field investigation confirms that the eastern boundary fault does exist, but it is a reverse fault characterized by sinistral motion rather than a normal fault. This fault, extending NE-SW on the whole, passes through Weijia, Haihui, Bailu, Hujiazui and Hualin and almost overlaps with the Wuli normal fault. To avoid confusion, we call it the Xingzi reverse fault. The Xingzi reverse fault can generally be divided into two segments, namely, the northern segment and the southern segment (division point at Haihui). The northern segment extends northward via Haihui, Zhoujiacun, and Fujiashan and then turns northeastward. The Liantuo Formation crops out to the west of this fault, while the Sinian, Cambrian and Silurian formations crop out to the east. Cretaceous granite and granodiorite intrusions are distributed along the fault. The extension direction of the southern segment is stable. The Neoproterozoic Xingzi Group is exposed to the west of the fault, while Cambrian and Silurian rocks are exposed to the east. The northern segment of the reverse fault is located on the piedmont and leaves no fault cliffs. The southern

segment of the reverse fault is far from the block mountain. The distance is approximately 4 km at Bailu and approximately 6 km at Liaohua. The distance roughly increases southward.

The outcrops of the Xingzi reverse fault are poor due to extensive cover by Quaternary deposits and the weathering crust. However, the fault crops out well at Hujiazui and Daao due to recent excavation. The Hujiazui profile (N29°24′22.9″, E116°0′7.41″) shows that the fault zone has a large scale with a visible width of approximately 80 m. To the east of the fault zone, Cambrian siltstone is exposed and to the west, the Neoproterozoic Xingzi Group (Figure 4). The fault zone is composed of two crushed zones intercalating one breccia zone. The rock blocks in the crushed zones are mainly Cambrian siltstone, and those in the breccia zone are mainly silicalite, quartz sandstone, siltstone, quartzite and leptynite. The breccia zone is wide at the top and tends to become narrow downward. The fault zone generally trends NE-SW. The interface between the Xingzi Group and the fault zone inclines to the west with a dip angle of approximately 45°. Therefore, the Xingzi Group to the west of the fault forms the hanging wall, while the Cambrian rocks to the east constitute the footwall. Because the Neoproterozoic Xingzi Group overlies the Cambrian units, this is clearly a reverse fault.

The exposure of the Xingzi reverse fault at Daao (N29°31′12.3″, E116°3′25.81″) is relatively poor. Silurian siltstone is exposed to the east of the fault zone, and the Neoproterozoic Xingzi Group is exposed to the west (Figure 5). The fault zone has a visible width of approximately 300 m and extends NE-SW. The interface between the Xingzi Group and the fault zone dips WNW at an angle of approximately 50°. Therefore, the Xingzi Group to the west of the fault forms the hanging wall, and the Silurian rocks to the east constitute the footwall, indicating that the Xingzi Group thrusts eastward and overrides the Silurian. The visible part of the fault zone is actually a breccia zone, which mainly contains blocks of silicalite, quartzite and mylonite in the western part and blocks of limestone in the eastern part. The mylonite probably comes from the ductile shear zone in the Xingzi Group, which demonstrates that the activity along this reverse fault occurred later than the ductile shear zone.

Both the Hujiazui and Daao profiles reveal that the Xingzi reverse fault is the eastern boundary fault of Lu Mountain. The Xingzi Group in the hanging wall thrusts eastward and overrides the Palaeozoic strata, which may also be the cause of incomplete Palaeozoic exposure on the eastern piedmont of Lu Mountain. The Xingzi reverse fault is characterized by a thick fault zone and is composed of crushed zones and breccia zones. The fault breccias coming from the Xingzi Group and the Palaeozoic rocks have been consolidated. The extensively developed fracture zone and the breccia zone should be the results of strong compression along the thrust fault. Interestingly, the fault zone forms a positive landform at both sites, which indicates not only that the fault was active early and the hanging wall has experienced long-term denudation but also that the Xingzi Group is more vulnerable to denudation than the Palaeozoic rocks. The reason why the Xingzi Group is easily denuded is that crystalline metamorphic rocks and extensively developed ductile shear zones are favourable for weathering. Other geological and geomorphic evidence also indicates that
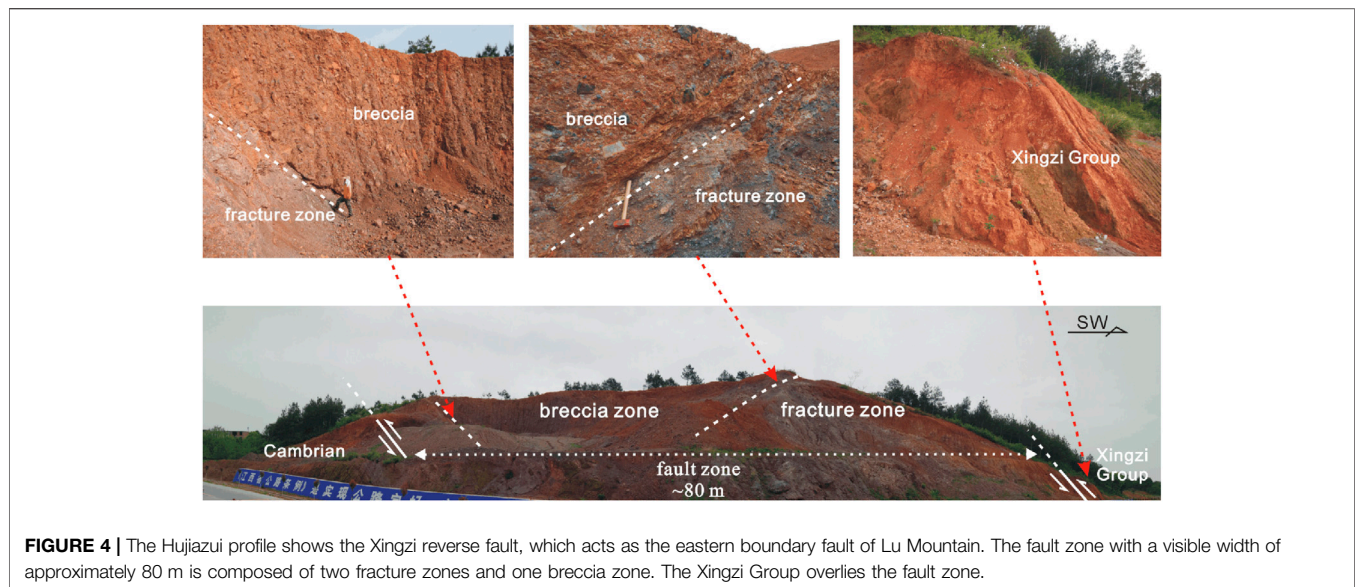
FIGURE 4 | The Hujiazui profile shows the Xingzi reverse fault, which acts as the eastern boundary fault of Lu Mountain. The fault zone with a visible width of approximately 80 m is composed of two fracture zones and one breccia zone. The Xingzi Group overlies the fault zone.
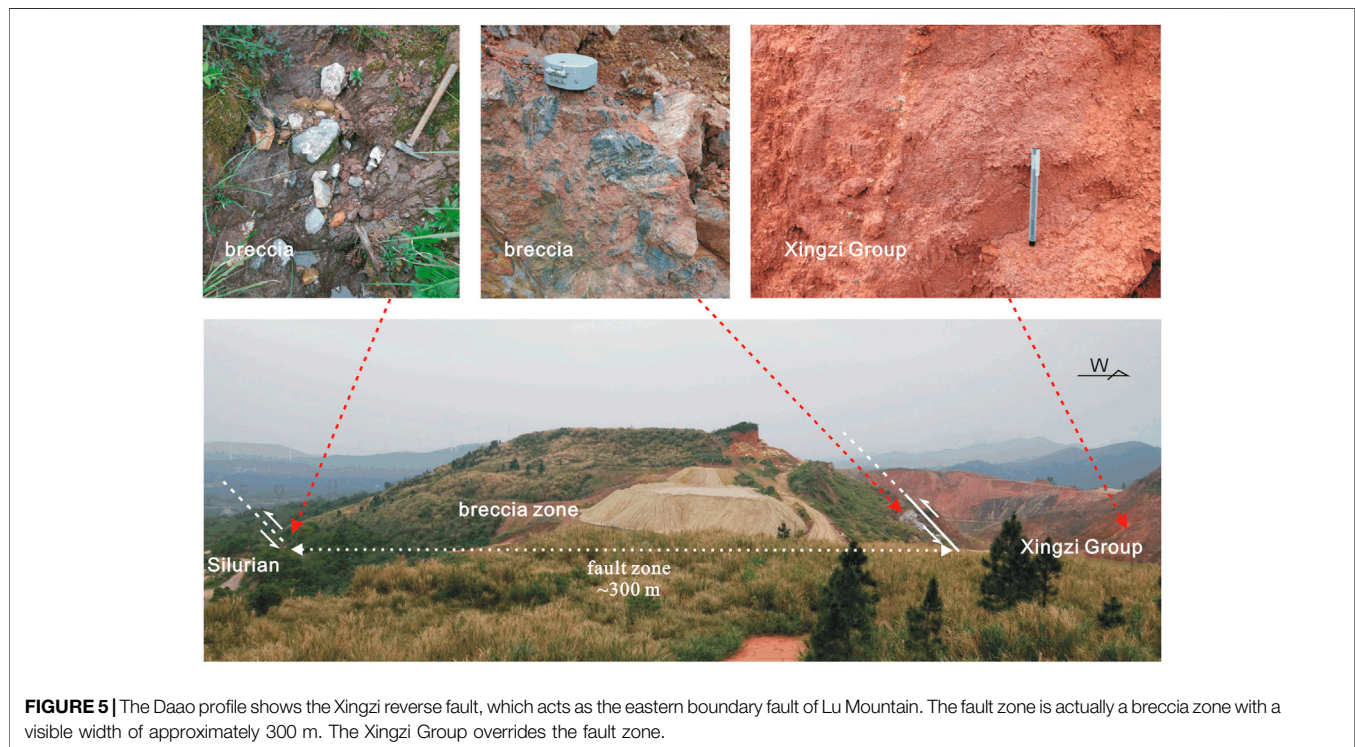

FIGURE 5 | The Daao profile shows the Xingzi reverse fault, which acts as the eastern boundary fault of Lu Mountain. The fault zone is actually a breccia zone with a visible width of approximately 300 m. The Xingzi Group overrides the fault zone.

the Xingzi reverse fault was active early: 1) the fault breccia is consolidated; 2) no Quaternary dislocation implies that the fault was probably active before the Quaternary; and 3) no fault valley or fault cliff suggests that the topographic relief produced by the fault was eliminated by long-term denudation.

Fan-Shaped Terrains

The landform of the eastern piedmont of Lu Mountain is characterized by the development of granitic monadnocks and fan-shaped terrain. In the core of the brachy-anticline, four large granitic monadnocks are exposed, namely, Donggushan (540 m a.s.l.), Xigushan (330 m a.s.l.), Yujingshan (324 m a.s.l.) and Hongmaojian (185 m a.s.l.) (**Figure 1C**). The Xingzi Group is exposed on the tops of these monadnocks. This fact shows that the granitic rocks have stronger resistance to erosion than the metamorphic rocks of the Xingzi Group. When the rocks surrounding the Xingzi Group are gradually eroded, the granitic intrusion becomes a monadnock.

Three fan-shaped terrains at different elevations have developed in the region from Haihui to Xingzi (**Figure 1D**).
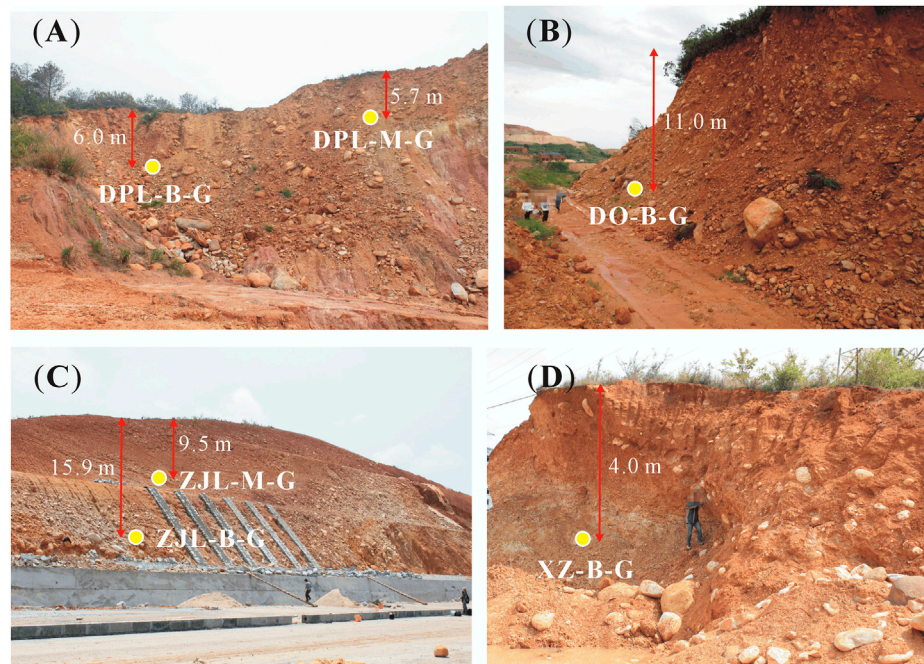
FIGURE 6 | Photographs show the sediments on the fan to the east of Lu Mountain and the sampling locations. **(A)** Colluvium at Dapailing. **(B)** Debris flow deposits at Daao. **(C)** Alluvium at Zhangjialong. **(D)** Debris flow deposits at Xingzi.

The low-level fan (Wanshancun fan) has elevations of approximately 45–20 m and extends from Wanshancun to the shore of Poyang Lake. This fan is surrounded by Donggushan, Hongmaojian and Yujingshan. The surface of this fan is relatively flat, and the Sanxia River flows southward on it. The middle-level fan (Xingzi fan) has elevations of approximately 70–30 m and is delimited by Yujingshan, Jindingshan, and Dalingshan. The ravine incision on this fan is not severe, and the outline of this low-relief fan remains relatively complete. The high-level fan (Dapailing fan) covers an area including Paishanling (252 m a.s.l.), Dapai Mountain (284 m a.s.l.), Changling (127 m a.s.l.), Dalingshan (149 m) and Jindingshan (193 m a.s.l.). Intense incision by ravines on this fan results in moderate relief. The hill tops within this fan may represent the original surface of the fan, probably the primitive piedmont denudation surface.

The deposits on the middle-level fan mainly comprise vermiculated diamicton and vermiculated laterite (Li et al., 1983), which were assigned to the middle Pleistocene Yejialong Formation (Xie et al., 1994). The Xingzi profile (N29°28′18.82″, E116°1′57.31″, 63 m a.s.l.) exposes brown-red vermiculated diamicton with a visible thickness of approximately 5 m (**Figure 6D**). Gravels supported by the matrix in the diamicton vary from less than 1 cm to 1 m in diameter and are presumed to be debris flow deposits. Deposits on the high-level fan were assigned to the early Pleistocene Dapailing Formation (Xie et al., 1994). The thickness of deposits on this fan varies greatly, and deposits at Dapailing, Daao and Zhangjialong are relatively thick. The diamicton in the Dapailing profile (N29°31′32.95″, E116°3′3.52″, 258 m a.s.l.) can be divided into two layers with a gradational contact: an upper brown-red layer and a lower greyish yellow layer.

The diamicton with a total thickness of approximately 6 m overlies the Xingzi Group. A grain-supported texture can be seen in the poorly sorted diamicton with gravels of size from several centimetres to 4 m. The main lithologies of the gravels include schist, quartz sandstone, leptynite, quartzite, and gneiss. Most gravels are sub-angular in shape, and the diamicton is assumed to be colluvium (**Figure 6A**). The Daao section (N29°31′20.47″, E116°3′17.18″, 186 m a.s.l.) exposes brown-red diamicton, with its color fading upward. The diamicton is approximately 10 m thick and covers the Xingzi reverse fault zone. The sizes of grain-supported gravels range from several centimetres to approximately 1 m. Schist and quartz sandstone gravels are common, and most of them are sub-angular. This diamicton is presumed to represent debris flow deposition (**Figure 6B**). The Zhangjialong profile (N29°30′34.48″, E116°3′14.32″, 90 m a.s.l.) exposes sandy gravel with a thickness of approximately 16 m. The sediments can be divided into three horizons: a red upper horizon, a brown-red middle horizon with vermiculated structure, and a grey-white or grey-yellow lower horizon with unclear vermiculated structure. The sizes of most gravels are 1–10 cm and rarely up to 50 cm. The grain-supported gravels are mainly rounded and sub-rounded in shape. These gravels are presumed to be the channel deposits of mountain rivers (**Figure 6C**).

Most samples for burial dating were selected from the bottoms of the sections. One sample (XZ-B-G) was taken from the Xingzi section, and another (DO-B-G) was taken from the Daao section. Two parallel samples (DPL-M-G and DPL-B-G) were taken from the Dapailing section. The position of sample DPL-M-G is relatively high, and the distance between the two samples is approximately 20 m. Samples were collected from the middle

TABLE 1 | Sample information and Al contents in quartz.

Sample	Site	Longitude and latitude	Elevation (m)	Depth (m)	Al content (ppm)	Quartz weight (g)
DPL-M-G	Dapailing	E116.051°, N29.526°	260	5.7	41.2	67.13
DPL-B-G	Dapailing	E116.051°, N29.526°	256	6.0	18.6	59.76
DO-B-G	Daao	E116.055°, N29.522°	186	11.0	47.5	44.75
ZJL-M-G	Zhangjialong	E116.054°, N29.509°	90	9.5	31.9	60.02
ZJL-B-G	Zhangjialong	E116.054°, N29.509°	90	15.9	38.5	56.55
XZ-B-G	Xingzi	E116.033°, N29.471°	63	4.0	39.7	49.12
QS-B-G	Qingshan	E119.056°, N32.263°	40	7.0	17.6	73.18

TABLE 2 | Contents of ^{26}Al and ^{10}Be in quartz samples.

Lab number	Sample	^{26}Al content (atoms/g)	Error (%)	^{10}Be content (atoms/g)	Error (%)
201,501,852	DPL-M-G	136,238 ± 7622	5.6	24,334 ± 1049	4.3
201,501,853	DPL-B-G	210,224 ± 8376	4.0	39,306 ± 1373	3.5
201,501,854	DO-B-G	205,625 ± 10,545	5.1	42,526 ± 1521	3.6
201,501,855	ZJL-M-G	211,600 ± 7892	3.7	51,442 ± 1563	3.0
201,501,856	ZJL-B-G	161,493 ± 7532	4.7	35,792 ± 1794	5.0
201,501,857	XZ-B-G	420,375 ± 15,873	3.8	104,179 ± 2334	2.2
201,501,858	QS-B-G	247,917 ± 7530	3.0	48,902 ± 1452	3.0

horizon (ZJL-M-G) and from the lower horizon (ZJL-B-G) in the Zhangjialong section (**Figure 6**). Each sample was composed of 20–30 gravels with diameters of several centimetres, and the selected gravels were either quartzite or vein quartz. To test the reliability of burial dating, one sample (QS-B-G) was also collected from the Qingshan section at Yizheng, Jiangsu (N32°15′40.06″, E119°3′19.13″, 36.3 m a.s.l.). The Qingshan section exposes a 2-m-thick sandy gravel covered by a 6-m-thick layer of Xiashu loess. The sample came from the sandy gravels of the Yuhuatai Formation (Han et al., 2009). Palaeomagnetic surveys demonstrated that the bottom age of the Xiashu loess is approximately 0.9 Ma (Li et al., 2018), so the sedimentary age of sample QS-B-G should be slightly greater than 0.9 Ma.

Burial Ages
The aluminum contents of the extracted quartz particles are low, ranging from 17.6 to 47.5 ppm. The acquired pure quartz samples weigh between 45 and 73 g (**Table 1**). The measured ^{26}Al and ^{10}Be contents indicate that the relative errors of the ^{26}Al contents are between 3.0% and 5.6% and that those of the ^{10}Be contents are between 2.2% and 5.0% (**Table 2**). The errors of ^{26}Al and ^{10}Be contents are so small that high-precision burial dating is possible. The ^{26}Al/^{10}Be dating results show that the uncorrected burial age (minimum burial age) of the Yuhuatai Formation sample from the Qingshan profile (QS-B-G) is 0.65 ± 0.10 Ma and that the corrected age (maximum burial age) increases to 1.04 ± 0.10 Ma, which is approximately 1.6 times larger than the uncorrected age. The ^{26}Al and ^{10}Be produced after burial ($N_{26,pb}$ and $N_{10,pb}$) are 2.6 times and 2.0 times greater than the ^{26}Al and ^{10}Be produced

before burial ($N_{26,inh}$ and $N_{10,inh}$), respectively. The uncorrected age is significantly less than the bottom age of the overlying Xiashu loess (0.9 Ma). In contrast, the corrected age is close to the bottom age and in line with the stratigraphic sequence (**Table 3**). This result indicates that the samples with insufficient burial depth must be corrected and that the corrected age may be regarded as the actual burial age.

Unfortunately, three samples from the Dapailing and Xingzi sections cannot be corrected, and only the minimum burial age can be given (**Table 3**). The minimum burial age of sample XZ-B-G from the Xingzi profile is 1.08 ± 0.10 Ma, and that of the parallel samples (DPL-M-G and DPL-B-G) is approximately 0.5 Ma. The ages of the samples from the middle and lower horizons in the Zhangjialong profile are out of sequence. The ^{26}Al and ^{10}Be produced ($N_{26,pb}$ and $N_{10,pb}$) after burial in the sample (ZJL-M-G) from the middle horizon are 9.8 and 4.7 times greater than the ^{26}Al and ^{10}Be inherited ($N_{26,inh}$ and $N_{10,inh}$) from before burial, respectively (**Table 3**). The corrected age (2.40 ± 0.11 Ma) is approximately 2.2 times larger than the uncorrected age (1.06 ± 0.11 Ma). More ^{26}Al and ^{10}Be produced after burial may lower the reliability of corrected ages. Therefore, the burial age of this sample is not used for further analysis.

The contents of ^{26}Al and ^{10}Be ($N_{26,pb}$ and $N_{10,pb}$) produced after burial in the sample (ZJL-B-G) from the lower horizon in the Zhangjialong profile are relatively low, and the corrected age (1.22 ± 0.15 Ma) is only 1.4 times larger than the uncorrected age (0.88 ± 0.15 Ma). Similar to this sample, sample (DO-B-G) from the Daao profile has a difference between the uncorrected age (0.74 ± 0.13 Ma) and the corrected age (1.10 ± 0.14 Ma) that is insignificant (**Table 3**). Therefore, the corrected ages are used as the actual burial ages for these two samples.

Denudation Rate
The ^{26}Al/^{10}Be dating results suggest that the deposits on the middle-level and high-level fans are older than 0.45 Ma. Interestingly, although the sedimentary origins and elevations are different, deposits at Daao (186 m a.s.l.) and Zhangjialong (90 m a.s.l.) on the high-level fan have similar burial ages, which indicates that both deposits may belong to heterofacies deposited during the same period. Ancient mountain rivers left deposits in the Zhangjialong section, and the elevation of the nearby modern rivers is approximately 50 m. Therefore, the eroded thickness can be estimated as approximately 40 m in the past 1.2 Myr, resulting in a denudation rate of approximately 0.033 m/kyr. Ancient debris flows left deposits in the Daao profile, and the elevation

TABLE 3 | ^{26}Al/^{10}Be burial ages (minimum burial ages) and corrected ages (maximum burial ages) by considering insufficient burial depth.

Sample	Surface production rate of ^{26}Al (atoms/g/yr)	Surface production rate of ^{10}Be (atoms/g/yr)	Minimum burial age (Ma)	$N_{26,pb}$ content (Atoms/g)	$N_{10,pb}$ content (Atoms/g)	$N_{26,inh}$ content (Atoms/g)	$N_{10,inh}$ content (Atoms/g)	Maximum burial age (Ma)
DPL-M-G	31.870	4.676	0.45 ± 0.15					Uncorrectable
DPL-B-G	31.767	4.666	0.54 ± 0.12					Uncorrectable
DO-B-G	30.108	4.421	0.74 ± 0.13	130,114 ± 1115	23,937 ± 60	75,511 ± 3926	18,589 ± 667	1.10 ± 0.14
ZJL-M-G	27.916	4.095	1.06 ± 0.11	192,136 ± 2793	42,407 ± 204	19,464 ± 779	9036 ± 278	2.40 ± 0.11
ZJL-B-G	27.916	4.095	0.88 ± 0.15	86,904 ± 809	16,307 ± 45	74,590 ± 3547	19,484 ± 978	1.22 ± 0.15
XZ-B-G	27.301	4.003	1.08 ± 0.10					Uncorrectable
QS-B-G	27.584	4.041	0.65 ± 0.10	179,881 ± 1475	32,676 ± 77	68,037 ± 2140	16,226 ± 483	1.04 ± 0.10
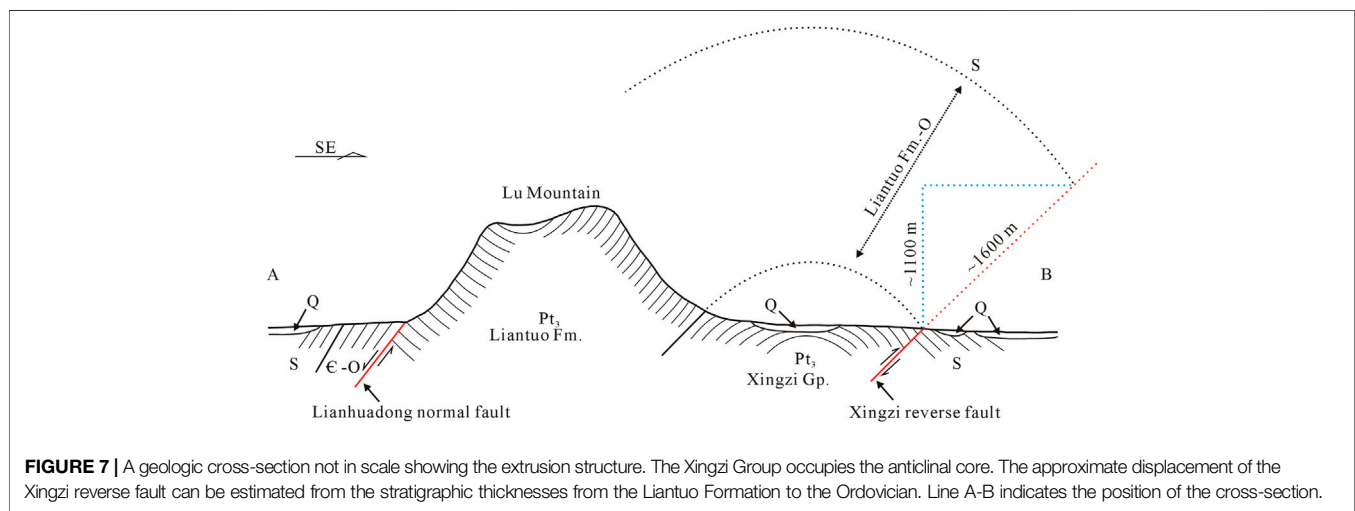
FIGURE 7 | A geologic cross-section not in scale showing the extrusion structure. The Xingzi Group occupies the anticlinal core. The approximate displacement of the Xingzi reverse fault can be estimated from the stratigraphic thicknesses from the Liantuo Formation to the Ordovician. Line A-B indicates the position of the cross-section.

of the nearby modern ravines is approximately 96 m. The eroded thickness can also be estimated as approximately 90 m, resulting in a denudation rate of 0.082 m/kyr.

The above results indicate that the denudation rate of the eastern piedmont of Lu Mountain has been between 0.033 and 0.082 m/kyr in the past 1.2 Myr. These data can be used to estimate the age of faulting along the Xingzi reverse fault. According to the 1:50,000 geological map of Haihui region (Jiangxi Bureau of Geology and Mineral Resources, 1993b), the thickness of the strata from the Nanhua System to the Ordovician is approximately 1,600 m (**Figure 7**). Since the fault is located on the east limb of the Lu anticline, the strata in this area are inclined to the ESE. We assume that the Xingzi reverse fault dips WNW at a 45° angle and that the strata are perpendicular to the fault. Now, the Xingzi Group has been elevated to contact the Silurian rocks, and the vertical fault displacement is at least 1,100 m. Such a large fault displacement must have produced a significant difference in elevation between the hanging wall and the footwall. However, there is no such topography along the southern segment of the Xingzi reverse fault, indicating that the high relief has been basically eliminated after long-term denudation. Therefore, the age of faulting should be older than or equal to the time required for eroding 1,100 m of rocks. The larger denudation rate (0.082 m/kyr) yields a denudation time of 13 Myr, while the

smaller rate (0.033 m/kyr) yields a denudation time of approximately 33 Myr. These data suggest that the Xingzi reverse fault was active in the Miocene or earlier.

DISCUSSION

Tectonic Style of the Block Mountain

The nature of the boundary fault is related to determining the tectonic pattern of Lu Mountain. A metamorphic core complex (Xiang et al., 1993) and an uplift-slip structure (Bi et al., 1998) have been suggested partly due to the existence of the Wuli normal fault to the east of Lu Mountain. The Wuli normal fault was originally found by analysing a drill core from Wuli. The fault inclines to the ESE and consists of fault breccia and fault gouge with thicknesses of 1–7 m (Xiang et al., 1993). The Wuli normal fault is obviously different from the Xingzi reverse fault. The Xingzi reverse fault has a larger scale, and its fracture zone is more than tens of meters. Therefore, the Wuli normal fault is speculated to be a secondary fault adjacent to the main fault, similar to a back-thrust fault.

Since the eastern boundary fault is a reverse fault, the block mountain is neither a horst nor a metamorphic core complex (nor an uplift-slip structure) because all of these geological structures require the presence of a normal fault inclined to the ESE in the

eastern piedmont of Lu Mountain. In fact, Lu Mountain is one part of a very large anticline that extends from Jiugong Mountain to Lu Mountain, as shown on the geological map (**Figure 2A**). In the vicinity of Jiugong Mountain, the fold axis is oriented W-E. Neoproterozoic rocks lie at the core of the anticline, and Sinian-Palaeozoic rocks make up the fold limb. To the east of Wuning, the southern limb of the anticline is partially covered by Cenozoic deposits or damaged by faulting. Near Dean, the northern limb of the anticline is also incomplete due to faulting, where the fold hinge turns northeast and gradually plunges (**Figure 2A**). The anticline is affected by both faulting and later denudation at Lu Mountain; as a result, the Nanhua System and the Sinian units on the southern limb are almost absent. The eastern and western boundary faults have severely disrupted the anticline.

The block mountain is actually bordered by the Lianhuadong normal fault in the west and the Xingzi reverse fault in the east, and both faults dip WNW (**Figure 7**). It is clear that the block mountain is situated on the upthrown sides of these two boundary faults. Numerical simulation shows that under a compressive regime, normal and reverse faults with the same dip direction can develop synchronously and thus form a vertical extrusion structure (Zeng et al., 2001). A similar geological structure appears in the Himalayan orogenic belt. The central thrust fault to the south of the high Himalayan crystalline series dips northward, and the Rongbusi normal fault to the north also dips northward (Burchfiel and Royden, 1985). Therefore, the high Himalayan crystalline series is considered a wedge extruded vertically between the normal and reverse faults (Hodges et al., 1993). Since Lu Mountain exhibits similar tectonic characteristics, it is reasonable to deduce that the tectonic style of Lu Mountain is a vertical extrusion structure.

Although new evidence contradicts the interpretation that Lu Mountain is a horst block mountain, it is still a block mountain. The margin of a typical block mountain is close to the boundary fault, and fault cliffs are sometimes visible. In contrast, the southeastern margin of Lu Mountain is far from the boundary fault.

The Poyang Lake basin is located east of Lu Mountain (**Figure 1B**). Previously, they were believed to be separated by a normal fault, with the Poyang Lake basin on the hanging wall. Therefore, the Poyang Lake basin was also regarded as a fault basin (Liu, 1987; Deng et al., 2003). In fact, a fault basin surrounded by normal faults is usually the product of crustal extensional deformation. Therefore, a fault basin is often regarded as an indicator of an extensional stress field (Wu et al., 2007). However, the discovery of the Xingzi reverse fault suggests that the Poyang Lake basin is a fault basin formed not by extensional deformation but by compressional deformation. Many Mesozoic or Cenozoic basins also have developed in East China. This study shows the possibility that some basins may have similar origins. To avoid misinterpretation of the tectonic stress field due to mistaking the fault basin, the properties of the basin-controlling fault must be further checked.

Activity History of the Xingzi Reverse Fault

The $^{40}Ar/^{39}Ar$ ages of different rocks in Lu Mountain are concentrated in the range of 100–140 Ma, indicating that a major cooling event occurred during the Cretaceous (Lin et al., 2000), which should be related to the tectonic uplift of Lu Mountain. Magmatic rocks are distributed in the core of the Lu anticline and along the Xingzi reverse fault, and the magmatic intrusion should have been synchronous with the development of the extrusion structure. The age of the syntectonic granodiorite suggests that the Lu anticline was formed at 127–133 Ma, and the granite intrusion along the fault indicates that the fault was formed at 100–110 Ma (Lin et al., 2000). Hence, the Xingzi reverse fault developed on the basis of the anticline.

The Ganjiang fault in Jiangxi Province can be regarded as the southern extension of the Tanlu fault (Wu et al., 2007), and the Xingzi reverse fault is located at the northern end of the Ganjiang fault. Therefore, the Tanlu fault and the Ganjiang fault may form the Xingzi reverse fault to some extent. The Ganjiang fault controls a series of Late Cretaceous-Palaeogene red beds in sedimentary basins. Structural and sedimentary features indicate that the activity of the Ganjiang fault reached its peak during the Mesozoic-Cenozoic (Deng et al., 2003). The Tanlu fault does not cut through Miocene volcanic rocks, indicating that the Tanlu fault was no longer active after the Neogene. The simulation of apatite fission track data shows that the Tanlu fault was uplifted rapidly at 70–60 Ma and approximately 10 Ma (Wang et al., 2007). The above study suggests that the Tanlu fault was active in the Cretaceous, dormant in the Palaeogene, and active again in the Miocene and became dormant again after this time.

The results of studies on river landform also confirm that the uplift of Lu Mountain has been episodic. The channel steepness derived from the stream power river incision model suggests that the uplift rate of Lu Mountain has undergone several changes, from slow uplift in the early stage to rapid uplift in the late stage (Han et al., 2017). In the early stage, long-term denudation formed the mature topography represented by wide valleys in the central region of the mountain. In the late stage, strong headward erosion formed the youthful topography represented by V-shaped valleys on the mountain margin. When Lu Mountain was uplifted along the boundary fault, the base level of erosion was lowered significantly, resulting in the production of knickpoints at the mountain fringe. The knickpoints gradually migrated upstream and have risen to an elevation of approximately 1000 m at present (Wang et al., 2015). V-shaped valleys below the knickpoints and wide valleys above the knickpoints are seen. As the peripheral rivers continue their headward erosion, the central mature topography will gradually be diminished. Along the lines of Shahe, Guling and Dapailing, the distance between the two boundary faults is approximately 12 km, and the width of the residual mature topography is no more than 5 km; that is, mature topography with a width of approximately 7 km has been eroded. Undoubtedly, short-term denudation cannot eliminate mature topography.

Combining the above evidence, we suggest that the Lu Mountain was uplifted mainly in the Miocene. The tectonic uplift of Lu Mountain can be inferred to have undergone four stages. In Stage I, during the Cretaceous, tectonic movement was active, and the Lu anticline and the initial form of the extrusion structure developed. During Stage II in the Palaeogene, this region was relatively quiet in terms of tectonic activity, and the height of the mountain probably decreased due to

continuous denudation. In Stage III, during the Miocene, tectonic movement was reactivated, the mountain rose dramatically along the boundary faults, and the extrusion structure was finally shaped. In Stage IV, after the Miocene, this region became quiet again, the massif retreated, and the metamorphic basement was exposed due to continuous denudation. The reason why Lu Mountain was previously considered to have been uplifted significantly in the Quaternary is that the vermiculated laterites have been sharply dislocated by the boundary faults. The vermiculated laterite occurring in the wide valleys of Lu Mountain was once correlated to the Pleistocene vermiculated laterite on the piedmont. The former was uplifted by approximately 300 m (Peng and Huang, 1982) or 600–800 m (Zhu, 1995) to the present position by neotectonic movements. Even accounting for a minimum uplift of 300 m at the beginning of the middle Pleistocene, the erosion rate of the hanging wall would reach 0.38 m/kyr, and the retreat rate of the fault cliff at Dapailing would be as high as 4.17 m/kyr. Such high erosion and retreat rates are unreasonable. Thus, we suggest another explanation: that is, the vermiculated laterite in the wide valleys was not formed in the Pleistocene but in the Neogene. Vermiculated laterite could have developed under a humid and hot climate when the monsoon was extremely strong in the middle Pleistocene (Yin and Guo, 2006). The climate at this time was still unable to form vermiculated laterite in the wide valleys (Peng and Huang, 1982). However, the temperature in the Neogene was higher than that in the middle Pleistocene (Zachos et al., 2008), so forming vermiculated laterite at higher elevations was possible.

Background of Tectonic Uplift

The formation of the extrusion structure and the episodic tectonic uplift of Lu Mountain may have occurred in response to the movement of the Pacific plate. During the Early and Middle Triassic, the South China block was lodged between the Indosinian block and the North China block. Geological structure trending E-W were developed due to the S-N-trending compression caused by the collision of plates. In the early Yanshanian orogeny, the westward subduction of the Pacific plate led to a great transition of tectonic orientations in East China, resulting in the development of NE-SW-trending structures (Li et al., 2011). Tectonic deformation, mainly compressive folds, nappe structures and new tectonic landforms, was thus produced (Ge et al., 2014). The NE-SW-trending Lu anticline might have formed against this background.

In the Early Cretaceous, the subduction of the Pacific plate turned NNW toward the continental margin of East Asia (Maruyama and Send, 1986), compression was intensified in East China, and the activity of NNE-trending faults was strengthened (Deng et al., 2003). The tectonic movement in Lu Mountain became active. During the Late Cretaceous-Palaeogene, due to the subduction of the Kula plate under the Eurasian continent, some landmasses or seamounts on the oceanic crust collided with the East Asian continental margin (Mizutani and Yao, 1991), resulting in the emergence of a new subduction zone on the ocean side. Consequently, the subduction rate slowed, and the main compressive stress changed to NW-SE (Zhou and Li, 2000). Against this background, the tectonic movement in Lu Mountain became inactive.

During the Miocene, the rapid subduction and extrusion of the Philippine Sea plate with respect to the Eurasian plate led to the occurrence of compressive and torsional stress fields in East China (Suo et al., 2017). The tectonic movement in Lu Mountain became active again. After the Miocene, due to the influence of back-arc spreading and eastward retreat of the oceanic trench (Hong and Luo 1989), intra-continental extensional deformation occurred in East China (Ge et al., 2014), mainly NW-NE extension (Ren et al., 2002). The geological movement in Lu Mountain ceased again.

CONCLUSION

The corrected burial ages from ^{26}Al/^{10}Be dating indicate that the sediments on the high-level fans on the eastern piedmont of Lu Mountain were deposited at 1.1–1.2 Ma, implying that the denudation rate of the piedmont is between 0.033 and 0.082 m/kyr. Field investigation shows that the Xingzi reverse fault is the boundary fault to the east of Lu Mountain with a vertical displacement of at least 1,100 m. The time required to erode the hanging wall to its present position is 13–33 Myr. This result and previous evidences imply that Lu Mountain was uplifted mainly in the Miocene. This study also reveals that the uplift of Lu Mountain can be ascribed to the development of an extrusion structure, which was probably produced by compressional deformation in response to Pacific plate movement.

DATA AVAILABILITY STATEMENT

The original contributions presented in the study are included in the article/Supplementary Material, further inquiries can be directed to the corresponding author.

AUTHOR CONTRIBUTIONS

ZH and XL designed and directed this study. ZH also performed the calculation of burial ages. RP made DEM analysis. YL (4th author) and YL (5th author) made sample pretreatment. All authors participated field investigation and drafted the manuscript.

FUNDING

ACKNOWLEDGMENTS

REFERENCES

Bi, H., Tan, K., Wu, Q., and Zhang, Q. (1996). Orogenesis-basinogenesis in mount Lu-Poyang Lake in north Jiangxi. *Geol. Jiangxi* 10 (1), 3–12. (in Chinese with English abstract).

Bi, H., Xiang, X., and Zhu, Y. (1998). Lushan uplift Bedding-Delamination structure. *Geotectonica et Metallogenia* 22 (1), 21–28. (in Chinese with English abstract).

Burchfiel, B. C., and Royden, L. H. (1985). North-south extension within the convergent Himalayan region. *Geology* 13, 679–682. doi:10.1130/0091-7613(1985)13<679:NEWTCH>2.0.CO;2

Clark, M. K., Farley, K. A., Zheng, D., Wang, Z., and Duvall, A. R. (2010). Early Cenozoic faulting of the northern Tibetan Plateau margin from apatite (U-Th)/He ages. *Earth Planet. Sci. Lett.* 296 (1-2), 78–88. doi:10.1016/j.epsl.2010.04.051

Deng, P., Shu, L., Yang, M., Guo, Y., and Yu, X. (2003). Geological features and dynamic evolution of the Ganjiang fault in Jiangxi Province. *Geol. Rev.* 49 (2), 113–122. doi:10.3321/j.issn:0371-5736.2003.02.001 (in Chinese with English abstract).

Fang, H. (1959). Neotectonic movement in the middle and lower reaches of the Yangtze River. *Acta Geol. Sin.* 39 (3), 328–343. (in Chinese).

Fang, X., Dupont-Nivet, G., Wang, C., Song, C., Meng, Q., Zhang, W., et al. (2020). Revised chronology of central tibet uplift (lunpola basin). *Sci. Adv.* 6. doi:10.1126/sciadv.aba729810.1126/sciadv.aba7298

Gao, L., Huang, Z., Ding, X., Liu, Y., Zhang, C., Wang, Z., et al. (2012). The geochronological relationship between the shaojiwa formation and the Xingzi complex Group in northwestern Jiangxi and the constraints on zircon SHRIMP U-Pb age. *Acta Geosci. Sin.* 33 (3), 295–304. doi:10.1007/s11783-011-0280-z (in Chinese with English abstract).

Ge, X., Liu, J., Ren, S., and Yuan, S. (2014). The formation and evolution of the Mesozoic-Cenozoic continental tectonics in eastern China. *Geol. China* 41 (1), 19–38. doi:10.3969/j.issn.1000-3657.2014.01.002 (in Chinese with English abstract).

Granger, D. E., Holland, H. D., and Turekian, K. K. (2014). "Cosmogenic nuclide burial dating in Archaeology and Paleoanthropology," in *Treatise on geochemistry*. Second Edition (Oxford: Elsevier), 14, 81–97. doi:10.1016/B978-0-08-095975-7.01208-0

Granger, D. E., and Muzikar, P. F. (2001). Dating sediment burial with in situ-produced cosmogenic nuclides: theory, techniques, and limitations. *Earth Planet. Sci. Lett.* 188 (1-2), 269–281. doi:10.1016/S0012-821X(01)00309-0

Granger, D. E., and Smith, A. L. (2000). Dating buried sediments using radioactive decay and muogenic production of ^{26}Al and ^{10}Be. *Nucl. Instrum. Meth. B* 172 (1-4), 822–826. doi:10.1016/S0168-583X(00)00087-2

Guan, J., He, B., and Li, D. (2010). SIMS U-Pb dating of the detrital zircons from the Xingzi Group in Lushan area and its geological significance. *Geotectonica et Metallogenia* 34 (3), 402–407. doi:10.1017/S0004972710001772 (in Chinese with English abstract).

Han, Z., Li, X., Cheng, Y., and Yang, D. (2009). Evolution of sedimentary environment of Neogene gravel beds near Nanjing. *Quat. Sci.* 29 (2), 361–369. doi:10.3969/j.issn.1001-7410.2009.02.21 (in Chinese with English abstract).

Han, Z., Li, X., Wang, N., Chen, G., Wang, X., and Lu, H. (2017). Application of river longitudinal profile morphometrics to reveal the uplift of Lushan Mountain. *Acta Geologica Sinica - English Edition* 91 (5), 1644–1652. doi:10.3969/j.issn.1000-9515.2017.05.00710.1111/1755-6724.13403

Hodges, K. V., Burchfiel, B. C., Royden, L. H., Chen, Z., and Liu, Y. (1993). The metamorphic signature of contemporaneous extension and shortening in the central Himalayan orogen: data from the Nyalam transect, southern Tibet. *J. Metamorph. Geol.* 11 (5), 721–737. doi:10.1111/j.1525-1314.1993.tb00183.x

Hong, H., and Luo, H. (1989). Effects of west-Pacific subduction on tectonics of Eastern China. *Earthquake Res. China* 5 (4), 34–44. (in Chinese with English abstract).

Hsu, K. J., Sun, S., Li, J., Chen, H., Pen, H., and Sengor, A. M. C. (1988). Mesozoic overthrust tectonics in south China. *Geology* 16 (5), 418–421. doi:10.1130/0091-7613(1988)016<0418:MOTISC>2.3.CO;2

Jiangxi Bureau of Geology and Mineral Resources (1993b). *1:50,000 Haihui geological mapping*.

Jiangxi Bureau of Geology and Mineral Resources (1993a). *1:50,000 lushan geological mapping*.

Jiangxi Bureau of Geology and Mineral Resources (1995a). *1:50,000 mahuiling geological mapping*.

Jiangxi Bureau of Geology and Mineral Resources (1995b). *1:50,000 Xingzi geological mapping*.

Kong, P. (2012). Cosmogenic nuclide burial dating: theory and application. *Quat. Res.* 32 (3), 388–393. doi:10.3969/j.issn.1001-7410.2012.03.03 (in Chinese with English abstract).

Li, J., Zhang, L., Deng, Y., and Zhou, S. (1983). Quaternary environmental evolution and geomorphologic development in Lu Mountain. *Sci. China Ser. B* (8), 734–745. (in Chinese).

Li, J., and Zhu, J. (1987). Physiographic study of lushan. *Scientia Geol. Sin.* 7 (4), 306–315. (in Chinese with English abstract).

Li, S., Yu, S., Zhao, S., Liu, X., Gong, S., Suo, Y., et al. (2013). Tectonic transition and plate reconstructions of the east asian continental margin. *Mar. Geology. Quat. Geology.* 33 (3), 65–94. doi:10.3724/SP.J.1140.2013.03065 (in Chinese with English abstract).

Li, S., Zhang, G., Zhou, L., Zhao, G., Liu, X., Suo, Y., et al. (2011). The opposite Meso-Cenozoic intracontinental deformations under the superconvergence: rifting and extension in the North China Craton and shortening and thrusting in the South China Craton. *Earth Sci. Front.* 18 (3), 79–107. (in Chinese with English abstract).

Li, X., Han, Z., Lu, H., Chen, Y., Li, Y., Yuan, X., et al. (2018). Onset of Xiashu loess deposition in southern China by 0.9 Ma and its implications for regional aridification. *Sci. China Earth Sci.* 61, 256–269. doi:10.1007/s11430-017-9134-2

Lin, W., Faure, M., Monié, P., Schärer, U., Zhang, L., and Sun, Y. (2000). Tectonics of SE China: new insights from the lushan massif (Jiangxi Province). *Tectonics* 19 (5), 852–871. doi:10.1029/2000TC900009

Liu, C. (1987). Elementary research of the new tectonic movement of Lu Shan. *J. Cent. China Normal Univ.* 21 (4), 603–610. doi:10.2307/2546335 (in Chinese with English abstract).

Ma, L. (2002). *Geological atlas of China*. Beijing: Geological Publishing House.

Maruyama, S., and Send, T. (1986). Orogeny and relative plate motions: example of the Japanese Islands. *Tectonophysics* 127 (3-4), 305–329. doi:10.1016/0040-1951(86)90067-3

Mizutani, S., and Yao, A. (1991). Radiolarians and terranes: Mesozoic geology of Japan. *Episodes* 14, 213–216. doi:10.18814/epiiugs/1991/v14i3/003

Palumbo, L., Hetzel, R., Tao, M., and Li, X. (2011). Catchment-wide denudation rates at the margin of NE Tibet from in situ-produced cosmogenic 10Be. *Terra Nova* 23, 42–48. doi:10.1111/j.1365-3121.2010.00982.x

Palumbo, L., Hetzel, R., Tao, M., Li, X., and Guo, J. (2009). Deciphering the rate of mountain growth during topographic presteady state: an example from the NE margin of the Tibetan Plateau. *Tectonics* 28, doi:10.1029/2009TC002455

Peng, B., and Huang, R. (1982). On the influence of new tectonic movement on soil formation and evolution. *Acta Pedologica Sin* 19 (4), 323–330. (in Chinese with English abstract).

Reiners, P. W., and Brandon, M. T. (2006). Using thermochronology to understand orogenic erosion. *Annu. Rev. Earth Planet. Sci.* 34, 419–466. doi:10.1146/annurev.earth.34.031405.125202

Ren, J., Tamaki, K., Li, S., and Zhang, J. (2002). Late Mesozoic and Cenozoic rifting and its dynamic setting in Eastern China and adjacent areas. *Tectonophysics* 344 (3-4), 175–205. doi:10.1016/S0040-1951(01)00271-2

Ren, M. (1953). A preliminary study on the topography of Lu Mountain. *Acta Geogr. Sin.* 20 (1), 61–73. doi:10.11821/xb195301005 (in Chinese).

Shi, Z., Gao, L., Li, T., Ding, X., Wang, J., Huang, Z., et al. (2014). Zircon U-Pb isotopes dating of Hanyangfeng Formation in Lushan area and its geological significance. *Geol. China* 41 (2), 326–334. (in Chinese with English abstract).

Shu, L., and Wang, D. (2006). A comparison study of basin and range tectonics in the western north America and southeastern China. *Geol. J. China Universities* 12 (1), 1–13. doi:10.3969/j.issn.1006-7493.2006.01.001 (in Chinese with English abstract).

Suo, Y., Li, S., Cao, X., Li, X., Liu, X., and Cao, H. (2017). Mesozoic-Cenozoic inversion tectonics of East China and its implications for the subduction process of the oceanic plate. *Front. Earth Sci.* 24 (4), 249–267. doi:10.13745/j.esf.yx.2017-3-17 (in Chinese with English abstract).

Tapponnier, P., Zhiqin, X., Roger, F., Meyer, B., Arnaud, N., Wittlinger, G., et al. (2001). Oblique stepwise rise and growth of the Tibet Plateau. *Science* 294, 1671–1677. doi:10.1126/science.105978

Wang, C., Zhao, X., Liu, Z., Lippert, P. C., Graham, S. A., Coe, R. S., et al. (2008). Constraints on the early uplift history of the Tibetan Plateau. *Proc. Natl. Acad. Sci. USA* 105 (13), 4987–4992. doi:10.1073/pnas.0703595105

Wang, J., He, B., and Guan, J. (2013). Study on age and mechanism of the metamorphism of the Xingzi Group in the lushan area, Jiangxi Province. *Geotectonica et Metallogenia* 37 (3), 489–498. doi:10.3969/j.issn.1001-1552. 2013.03.013 (in Chinese with English abstract).

Wang, N., Han, Z., Li, X., Chen, G., Wang, X., and Lu, H. (2015). Tectonic uplift of Mt. Lushan indicated by the steepness indices of the river longitudinal profiles. *Acta Geogr. Sin.* 70 (9), 1516–1525. doi:10.11821/dlxb201509013 (in Chinese with English abstract).

Wang, X., Zhong, D., Zhang, J., Ji, J., and Wang, X. (2007). Low-temperature thermochronological constraints on sinistral strike-Slip movement of the Yi-Shu fault zone between the late Cretaceous and early Paleogene. *Acta Geol. Sin.* 81 (4), 454–465. doi:10.1016/S1872-5791(07)60044-X (in Chinese with English abstract).

Wu, G., Liang, X., and Chen, H. (2007). An approach to the Tancheng-Lujiang fault zone: its creation, evolution and character. *Chin. J. Geol.* 42 (1), 160–175. doi:10. 1016/S1872-5791(07)60044-X (in Chinese with English abstract).

Xiang, X., Xu, J., and Xu, K. (1993). Characteristics of metamorphic core complexes of Xingzi Group and its geological significance. *Miner. Resour. Geol.* 7 (6), 401–407. (in Chinese with English abstract).

Xie, G., Deng, B., Luo, C., and Huang, S. (1996). The establishment of Xingzi rock swarm in mount Lu area, Jiangxi and its geological significance. *Geol. Jiangxi* 10 (4), 274–279. (in Chinese with English abstract).

Xie, G., Feng, Y., and Ma, Z. (1994). The classification of the Quaternary lithostratigraphic unit in Lushan area. *Geol. Jiangxi* 8 (4), 272–280. (in Chinese with English abstract).

Xu, Y., Liang, Y., Jiang, S., Luo, M., Ji, J., Zhang, Z., et al. (2014). Evolution of cenozoic sedimentary basins in eastern China. *Earth Sci. – J. China Univ. Geosciences* 39 (8), 1079–1098. doi:10.3799/dqkx.2014.096 (in Chinese).

Yin, G., and Xie, G. (1996). Extensional structure and the Xingzi metamorphic core complex in the Lushan area. *Jiangxi. Region. Geol. China* (1), 17–26. (in Chinese with English abstract).

Yin, Q., and Guo, Z. (2006). The vermiculated laterite in South China reveals an unusually strong period of the East Asian monsoon. *Chin. Sci. Bull.* 51 (2), 186–193. doi:10.3321/j.issn:0023-074X.2006.02.01210.1007/s11434-005-0490-5 (in Chinese).

Yuan, D.-Y., Champagnac, J.-D., Ge, W.-P., Molnar, P., Zhang, P.-Z., Zheng, W.-J., et al. (2011). Late Quaternary right-lateral slip rates of faults adjacent to the lake Qinghai, northeastern margin of the Tibetan Plateau. *Geol. Soc. America Bull.* 123, 2016. doi:10.1130/B30315.1

Zachos, J., Dickens, G., and Zeebe, R. (2008). An early Cenozoic perspective on greenhouse warming and carbon-cycle dynamics. *Nature* 451, 279–283. doi:10. 1038/nature06588

Zeng, Z., Yang, W., Franz, N., Liu, L., and Guo, T. (2001). Extrusion tectonics in orogenic belt. *Geol. Sci. Tech. Inform.* 20 (1), 1–7. doi:10.3969/j.issn.1000-7849. 2001.01.001 (in Chinese with English abstract).

Zheng, W.-J., Zhang, P.-Z., Ge, W.-P., Molnar, P., Zhang, H.-P., Yuan, D.-Y., et al. (2013). Late quaternary slip rate of the south heli Shan fault (northern hexi corridor, NW China) and its implications for northeastward growth of the Tibetan plateau. *Tectonics* 32, 271–293. doi:10.1002/tect.20022

Zhou, X., and Li, W. (2000). Origin of Late Mesozoic igneous rocks in Southeastern China: implications for lithosphere subduction and underplating of mafic magmas. *Tectonophysics* 326 (3-4), 269–287. doi:10.1016/S0040-1951(00) 00120-7

Zhu, C. (1995). The new recognitions to genesis Quaternary sediments and neotectonics in the east piedmont of the Lushan Mountain. *Acta Geogr. Sin.* 50 (1), 41–50. doi:10.11821/xb199501005 (in Chinese with English abstract).

Zhu, Q., Yang, K., and Wang, Y. (2010). Extensional detachment and magmatism of the lushan metamorphic core complex: constraints from $^{40}Ar/^{39}Ar$ and U-Pb geochronology. *Geotectonica et Metallogenia* 34 (3), 391–401. doi:10.1017/ S0004972710001772 (in Chinese with English abstract).